

# Phases of the interacting one-dimensional electron gas coupled to phonons

Ian P. Bindloss

*Department of Physics, University of California, Los Angeles, California 90095-1547*

(Dated: December 2, 2024)

Using a multi-step renormalization group method, we study the zero-temperature phases of the interacting one-dimensional electron gas coupled to phonons. We compute the weak-coupling quantum phase diagram of the 1D extended Holstein-Hubbard model and the 1D extended Peierls-Hubbard model at half-filling and incommensurate filling. At incommensurate fillings, the phase diagrams are characterized by a delicate competition between spin density wave, charge density wave, and superconducting orders. We study the dependence of the ground state on the electron-phonon (el-ph) and electron-electron (el-el) coupling strengths, the screening length, electron bandwidth, phonon frequency, doping, and type of phonon band. The competition between ordering fluctuations is sensitive to all of the above. Unlike the case in Fermi liquids, in 1D the el-ph coupling is strongly renormalized, often to stronger values. Therefore, even when the bare phonon induced attraction is weak compared to the bare el-el repulsion, just a small amount of retardation makes it possible for the renormalized el-ph interaction to dominate the problem. The el-ph interaction can create a gap in the spin sector, and, in some cases, a strongly divergent superconducting susceptibility. We find that there are cases in which a repulsive el-el interaction enhances the superconducting susceptibility in the presence of a retarded el-ph interaction.

## I. INTRODUCTION

Recent experiments<sup>1</sup> in the high-temperature superconductors that point to a strong and ubiquitous electron phonon (el-ph) interaction have led to an increased interest in strongly correlated el-ph systems. Of particular interest is the interplay between the repulsive, instantaneous Coulomb interaction and the attractive, retarded interaction mediated by phonons, in the context of various phase transitions (instabilities) of the system. This interplay is quite simple and well understood in a two or three dimensional Fermi liquid, and serves as a foundation for the BCS theory of superconductivity. However, the high-temperature superconductors, as well as some other materials of current interest, exhibit manifestly non-Fermi liquid behavior.<sup>2,3,4,5,6</sup>

Compared to conventional metals, much less is known about the influence of an el-ph interaction in non-Fermi liquids. One such system, where much analytic progress can be made,<sup>7,8,9</sup> is the interacting one-dimensional electron gas (1DEG). In contrast to higher dimensions, in one-dimension (1D) the el-ph interaction is strongly renormalized. In other words, the effective el-ph interaction at low energies is not simply given by the bare, microscopic coupling constants, which makes the physics both very different and very rich. Furthermore, the renormalizations of the el-ph interactions are affected by direct electron-electron (el-el) interactions. It is unknown how much of the physics of the 1DEG is generic to other non-Fermi liquids; but one may hope that certain features are generic, in which case the 1DEG may serve as a paradigmatic model for a broader class of systems. In addition, there are many reasons to study the 1DEG coupled to phonons for its own sake, including the importance of el-ph interactions in the quasi-1D conducting polymers,<sup>10</sup> and the possibility that they play an important role in the quasi-1D organic conductors.<sup>11</sup> It may

also be the case that holes in the high-temperature superconductors live in quasi-1D due to stripe correlations.<sup>12</sup> In any case, since in 1D a small bare el-ph coupling can be renormalized to substantially larger values, the el-ph interaction is important to consider.

In the present paper, we use a multi-step renormalization group (RG) procedure to comprehensively study the zero-temperature phase diagrams of the spinful 1DEG coupled to phonons, treating the el-el and el-ph interactions on equal grounds. In a separate paper,<sup>6</sup> we have studied the influence of the el-ph interaction on the electron dynamics of an interacting 1DEG, expressed via the single particle spectral function. The strategy in the present paper is to start with a microscopic electron-phonon model with many parameters (el-el interactions, electron bandwidth, el-ph interactions, and phonon frequency), and then to integrate out high energy degrees of freedom to produce a low energy effective field theory with a known phase diagram—the continuum 1DEG—whose only parameters are the renormalized el-el interactions and bandwidth. If the system is far from commensurate filling, this is accomplished in two steps:<sup>13,14</sup> One set of RG equations governs the flow of the coupling constants for energies  $\omega$  greater than the phonon frequency  $\omega_0$ , while a second set governs the flow for  $\omega_0 > \omega$ . If, as usual, the Fermi energy  $E_F \gg \omega_0$ , the first step is to integrate out degrees of freedom from  $E_F$  to  $\omega_0$  using the microscopic coupling constants as initial values. The resulting renormalized couplings are then used as initial values in the second stage of RG flows, to integrate out degrees of freedom from  $\omega_0$  to some low energy scale. Near half-filling, there are three steps to the RG transformation; defining  $\mu$  as the chemical potential relative to its value at half-filling, for  $\mu > \omega_0$  these steps are  $E_F > \omega > \mu$ , then  $\mu > \omega > \omega_0$ , and finally  $\omega_0 > \omega$ .

We apply this technique to two microscopic models of the el-ph interaction: the Holstein model<sup>15</sup> and the

Su-Schrieffer-Heeger (SSH) model<sup>16</sup>, both generalized to include extended Hubbard interactions. Following others, we henceforth refer to the SSH model as the Peierls model. Since the RG procedure is perturbative (one-loop), our results are strictly valid only for interactions that are small compared to the bandwidth, but are valid for any relative strength of the el-ph and el-el interactions. The method can be used for any phonon frequency, and therefore properly takes into account the quantum phonon dynamics. We are able to derive analytic expressions for various zero-temperature phase boundaries that are quantitatively accurate for weak interactions. Corrections at stronger couplings are expected to be smooth and should not make large qualitative changes to the results, as long as the interactions are not too large.

One question we address is whether singlet superconductivity can exist in realistic 1D systems in which the bare el-el repulsion is stronger than the bare attractive interaction mediated by the el-ph coupling. It is known that in the absence of el-ph interaction, a repulsive el-el interaction in a single chain 1DEG is always harmful to superconductivity, as is the case in higher dimensions. However, we find the surprising result that in an incommensurate 1DEG with a retarded el-ph interaction, adding el-el repulsion can in some specific cases enhance superconductivity. Moreover, with just a small amount of retardation, it is possible for a 1DEG to have a divergent superconducting susceptibility even when the bare el-el repulsive is much stronger than the bare el-ph attraction. (In 3D this is only possible with substantial retardation.)

The rest of this paper is organized as follows. Sec. II defines the microscopic models that we investigate in this paper. Sec. III presents the main results of our calculation, in the form of phase diagrams, without any derivation. In Sec. IV we briefly compare our results to the work of other authors. Sec. V discusses the scaling of the coupling constants and contains a mathematical derivation of the phase diagrams. In Sec. VI we make some concluding remarks and speculate on the possible relevance of our results to the high-temperature superconductors.

## II. MODELS OF 1D ELECTRON-PHONON SYSTEMS

The extended Peierls-Hubbard (Pei-Hub) model of interacting electrons coupled to phonons in 1D is given by the Hamiltonian

$$\begin{aligned} \mathcal{H}_{\text{Pei-Hub}} = & \\ & - \sum_{i,\sigma} [t - \alpha(u_{i+1} - u_i)] (c_{i,\sigma}^\dagger c_{i+1,\sigma} + \text{H.C.}) \\ & + \sum_i \left[ \frac{p_i^2}{2M} + \frac{\kappa}{2}(u_{i+1} - u_i)^2 \right] + \mathcal{H}_{UV} \end{aligned} \quad (1)$$

with

$$\mathcal{H}_{UV} = U \sum_i n_{i,\uparrow} n_{i,\downarrow} + V \sum_i n_i n_{i+1}. \quad (2)$$

In this model, acoustic phonons couple to electrons by modifying the bare hopping matrix element  $t$  by the el-ph coupling strength  $\alpha$  times the relative displacements  $u_{i+1} - u_i$  of two neighboring ions. The operator  $c_{i,\sigma}^\dagger$  creates an electron of spin  $\sigma$  on site  $i$ ,  $\kappa$  is the spring constant,  $M$  is the ion mass,  $p_i$  is the phonon momentum operator, and  $n_i = \sum_\sigma n_{i,\sigma} = \sum_\sigma c_{i,\sigma}^\dagger c_{i,\sigma}$ . For this model we will approximate the phonon dispersion by its value at the zone boundary of  $2\sqrt{\kappa/M} \equiv \omega_0$ , since the el-ph interaction vanishes at zero momentum transfer. The el-el interaction part  $\mathcal{H}_{UV}$  is that of the extended Hubbard model. In this paper we only explicitly discuss the case of repulsive el-el interactions ( $U, V > 0$ ), however the mathematics remains valid for attractive ones.

The 1D extended Holstein-Hubbard (Hol-Hub) model is defined by the Hamiltonian

$$\begin{aligned} \mathcal{H}_{\text{Hol-Hub}} = & \\ & -t \sum_{i,\sigma} (c_{i,\sigma}^\dagger c_{i+1,\sigma} + \text{H.C.}) + \sum_i \left[ \frac{p_i^2}{2M} + \frac{1}{2} M \omega_0^2 q_i^2 \right] \\ & + g \sqrt{2M\omega_0} \sum_i q_i n_i + \mathcal{H}_{UV}. \end{aligned} \quad (3)$$

In this model, a dispersionless optical phonon mode with vibrational coordinate  $q_i$  and frequency  $\omega_0$  couples to the local electron density with el-ph coupling strength  $g$ . Unlike the Pei-Hub model, this model contains equal parts backward scattering (momentum transfer near  $2k_F$ ) and forward scattering (momentum transfer near 0) el-ph interactions. Another difference is that the el-ph interaction is site centered (diagonal) in the Hol-Hub model versus bond centered (off-diagonal) in the Pei-Hub model.

For convenience we define the following dimensionless quantities:

$$\begin{aligned} \lambda_{\text{Pei}} = \frac{4\alpha^2 \sin^2 k_F}{\pi v_F \kappa}, \quad \lambda_{\text{Hol}} = \frac{2g^2}{\pi v_F \omega_0}, \\ \bar{U} = \frac{U}{\pi v_F}, \quad \bar{V} = \frac{V'}{\pi v_F}, \quad l_0 = \ln \left( \frac{E_F}{\omega_0} \right), \end{aligned} \quad (4)$$

where  $v_F$  is the Fermi velocity,  $V' = -V \cos(2k_F)$ , and  $E_F > \omega_0$  is a high energy cutoff for the RG theory on the order of the Fermi energy. At half-filling,  $v_F = 2t$ ,  $k_F = \pi/2$ , and  $V = V'$ . The el-ph coupling parameters  $\lambda_{\text{Pei}}$  and  $\lambda_{\text{Hol}}$  are defined such that, in the absence of el-el interactions, the spin gap is given by  $\Delta_s \propto \exp(-a/\lambda)$ , where  $a = 1/2$  for half-filling,  $a = 1$  for incommensurate fillings, and  $\lambda$  stands for  $\lambda_{\text{Pei}}$  or  $\lambda_{\text{Hol}}$ , depending on the model. (In Sec. V we give the result for  $\Delta_s$  in the presence of el-el interactions.) The method we employ yields phase diagrams that are quantitatively accurate for  $\lambda, \bar{U}, \bar{V} \ll 1$ . We expect that the technique is qualitatively accurate when these couplings are of order 1. It should be clear that, in the present paper, we have set the lattice parameter and Planck's constant equal to one.

### III. RESULTS FOR THE PHASE DIAGRAMS

In this section we present our main results for the phase diagrams, without derivation. More discussion of the method and a detailed derivation is given in Sec. V, where we provide explicit expressions for the phase boundaries.

#### A. Incommensurate filling

Below we present phase diagrams for strongly incommensurate filling, which corresponds to  $\mu \sim E_F$  (here the chemical potential  $\mu$  is far from its half-filled value of zero).

##### 1. Transition to a spin-gapped phase

For the 1D extended Hubbard model without el-ph interactions, the low energy properties are described by the spin-charge separated Luttinger liquid (LL) as long as  $\bar{V} < \bar{U}/2$ . This gapless, quantum-critical state of matter can be described by a bosonic free field theory,<sup>17,18,19,20</sup> and represents a line of fixed points for interacting electrons in 1D. Since the quasiparticle residue vanishes, the LL is by definition a non-Fermi liquid; there are no elementary excitations with the quantum number of an electron (or a hole).

In the absence of el-ph interactions, a spectral gap develops in the spin sector if  $\bar{V} > \bar{U}/2$ , which leads to quite different physical properties than the LL. This non-Fermi liquid phase is termed a Luther-Emery liquid<sup>21</sup> (LEL). However, in nature one typically expects  $\bar{V} < \bar{U}/2$ , so that some additional physics is needed to create a spin gap. For incommensurate fillings, the charge sector is always gapless.

We now study the effects of the el-ph interaction on the phase boundary between the LL and spin-gapped LEL. In Fig. 1 we show a phase diagram in the  $\bar{V} - \bar{U}$  plane, for various fixed values of  $\lambda$  and  $E_F/\omega_0$  (this phase boundary is the same for the Pei-Hub and Hol-Hub models). We see that a retarded el-ph interaction dramatically increases the stability of the LEL phase relative to the LL phase. The phase boundary is very sensitive to the retardation parameter  $E_F/\omega_0$ , with higher values favoring the LEL phase. For the case of an unretarded el-ph interaction ( $\omega_0 > E_F$ ), which is not typical in real materials, a spin gap can only occur for  $\lambda > \bar{U} - 2\bar{V}$ . Just a small amount of retardation makes a spin gap possible, even for  $\lambda \ll \bar{U} - 2\bar{V}$ . As we show in Sec. V, this is due to the renormalization of the backscattering el-ph interaction toward stronger values. The figure shows that poorly screened interactions (high  $\bar{V}/\bar{U}$ ) favor the LEL. The dependence of the phase boundary on  $\bar{V}/\bar{U}$  is shown explicitly in Fig. 2, which presents a phase diagram in the  $\lambda l_0 - \bar{U} l_0$  plane. This diagram shows that, for repul-

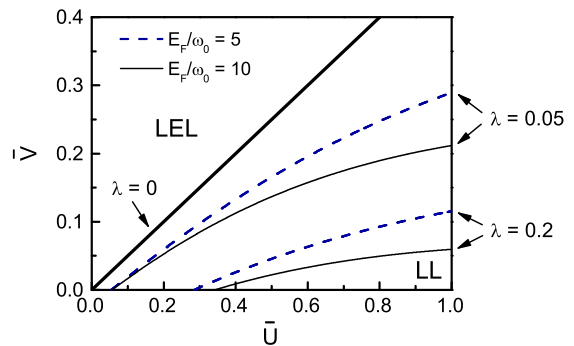


FIG. 1: Phase diagram in the  $\bar{V} - \bar{U}$  plane showing the  $\lambda$  dependence of the transition line between the gapless Luttinger liquid (LL) phase and the spin-gapped Luther-Emery liquid (LEL) phase, for an incommensurate 1DEG with  $E_F/\omega_0 = 5$  (dashed lines) and  $E_F/\omega_0 = 10$  (thin solid lines). The  $\lambda = 0$  transition line (thick line) is for any  $E_F/\omega_0$ . The electron-phonon coupling constant  $\lambda$  stands for  $\lambda_{\text{Hol}}$  or  $\lambda_{\text{Pei}}$ , depending on the model.

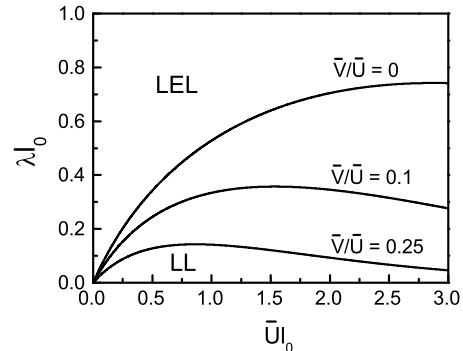


FIG. 2: Phase diagram in the  $\lambda l_0 - \bar{U} l_0$  plane for an incommensurate 1DEG, showing the dependence of the transition line between the gapless LL and spin-gapped LEL on the ratio  $\bar{V}/\bar{U}$ . Here  $\lambda$  stands for  $\lambda_{\text{Hol}}$  or  $\lambda_{\text{Pei}}$ , depending on the model, and  $l_0 \equiv \ln(E_F/\omega_0)$  parameterizes the retardation.

sive el-el interactions, scaling eventually carries one to the case in which an infinitesimal  $\lambda$  causes a spin gap.

##### 2. Competition between SDW, CDW, and superconductivity

Below, we explore the many ordering instabilities present in the system. We show that  $2k_F$  spin density wave order (SDW),  $2k_F$  charge density wave order (CDW), and singlet superconductivity (SS) can all compete at zero temperature. A divergent charge density wave susceptibility with  $4k_F$  periodicity (labeled in phase diagrams as “ $4k_F$ ”) is also possible. It is important to note that since long range order is forbidden in an incommensurate 1D system, the phase diagrams below actually consist of identifying instabilities with divergent response functions. However, for a quasi-1D array of weakly coupled chains, interchain coupling allows for true broken

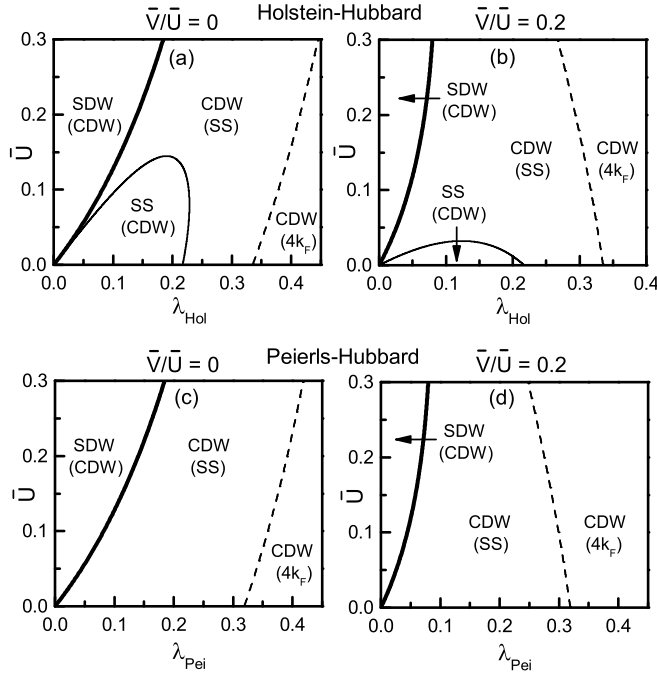


FIG. 3: Phase diagrams of the incommensurate extended Hol-Hub model for (a)  $V = 0$  and (b)  $\bar{V}/\bar{U} = 0.2$ , and of the incommensurate extended Pei-Hub model for (c)  $V = 0$  and (d)  $\bar{V}/\bar{U} = 0.2$ . The diagrams were computed for  $E_F/\omega_0 = 10$ . The charge sector is gapless everywhere in the diagrams. All parameter space to the right of the thick line is spin-gapped (the LEL). The most divergent susceptibility is shown without parenthesis, while parenthesis indicate a susceptibility that diverges less strongly. SDW stands for  $2k_F$  spin density wave, CDW stands for  $2k_F$  charge density wave, SS stands for singlet superconductivity, and  $4k_F$  stands for  $4k_F$  charge density wave.

symmetry order at low temperature.

In Fig. 3 we present phase diagrams in the  $\bar{U} - \lambda_{\text{Hol}}$  and  $\bar{U} - \lambda_{\text{Pei}}$  planes, for the case  $E_F/\omega_0 = 10$ . In these diagrams, we show phase boundaries between regions where various ordering fluctuations have divergent susceptibilities in the low temperature limit. The susceptibility that diverges most strongly, *i.e.* dominates, is shown without parenthesis. If a second susceptibility diverges, but less strongly, it is termed “sub-dominant,” and is shown in parenthesis. The thick solid line is the LL-LEL transition line; the LL phase is present to left of this line and the LEL phase to the right.

For repulsive el-el interactions, the entire LL phase, for either model, is dominated by SDW fluctuations, with a slightly weaker CDW susceptibility. The LEL phase is more complex. For the extended Hol-Hub model, dominant SS order is possible provided the el-el repulsion is weak enough and  $\lambda_{\text{Hol}}$  is neither too weak *nor* too strong. For the Pei-Hub model with repulsive el-el interactions, a phase with dominant SS is impossible due to the absence of el-ph forward scattering. Therefore, generally speaking, an optical phonon band is favorable to SS, while an

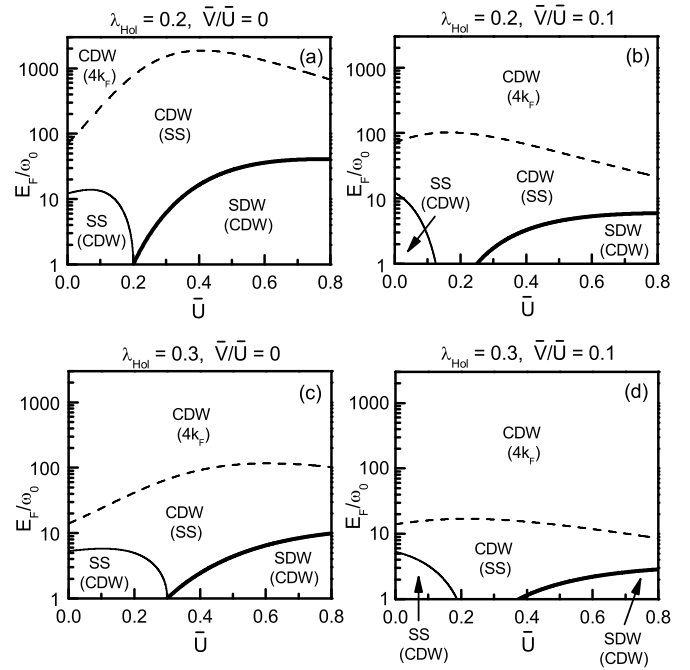


FIG. 4: Phase diagrams of the incommensurate extended Hol-Hub model. (a) and (b) are for  $\lambda_{\text{Hol}} = 0.2$ ; (c) and (d) are for  $\lambda_{\text{Hol}} = 0.3$ . (a) and (c) are for  $\bar{V}/\bar{U} = 0$ ; (b) and (d) are for  $\bar{V}/\bar{U} = 0.1$ . Parenthesis indicate a sub-dominant susceptibility. The region with dominant SDW is the LL phase, while the rest of the parameter space is a LEL.

acoustic band is not. In both models, there is a large region, for intermediate values of  $\lambda$ , with dominant CDW and sub-dominant SS. At high values of  $\lambda$ , SS is no longer divergent; in this region a  $2k_F$  CDW dominates and a  $4k_F$  CDW is sub-dominant. We must point out that the dashed line is not expected to be quantitatively accurate, since the method is a weak-coupling one. The thick and thin solid lines are quantitatively accurate at weak coupling.

Note the strong dependence of the phase diagram on the screening, expressed via the ratio  $\bar{V}/\bar{U}$ . The spin gap is enhanced by poor screening (large  $\bar{V}/\bar{U}$ ), but the phase with dominant SS is strongly suppressed by poor screening. However, decreasing the screening (increasing  $\bar{V}/\bar{U}$ ) can drive a LL to a LEL, thereby causing a divergent SS susceptibility where there was none before.

Although, generally speaking, increasing the el-el repulsion suppresses superconductivity, there are exceptions to this. For example, when  $\bar{V}/\bar{U} < 1/6$ , the effect of an el-el repulsion, in some cases, is to suppress the effective el-ph backscattering, which can enhance the SS susceptibility (this is discussed more in Sec. V). An example of this is as follows: we start at  $\lambda = 0.4$  and  $\bar{U} = 0$  in Figs. 3a or 3c, and increase  $\bar{U}$  while holding  $\lambda$  fixed, thereby moving from a phase without divergent SS to a phase with divergent SS! Such an enhancement of superconductivity by the el-el repulsion never occurs

for weak-coupling in conventional 3D metals.

We study the dependence of the ground state on  $E_F/\omega_0$  by showing phase diagrams in the  $E_F/\omega_0 - \bar{U}$  plane, for the Hol-Hub model, in Fig. 4. This figure illustrates that high values of  $E_F/\omega_0$  create a spin-gapped phase with dominant CDW. Low values of  $E_F/\omega_0$  create a SS dominated LEL for low  $\bar{U}$ , and a LL for high  $\bar{U}$ . In other words, an electron bandwidth that is too big is harmful to superconductivity! Note that for moderate  $E_F/\omega_0$ , the system lies in the region with dominant CDW and sub-dominant SS, which extends from  $\bar{U} = 0$  to quite large values of  $\bar{U}$ . Therefore, even when the bare interactions are predominantly repulsive ( $\bar{U} \gg \lambda_{\text{Hol}}$ ), it is still possible for the system to have a divergent superconducting correlation. It is possible for this to occur even with just a tiny amount of retardation like  $E_F/\omega_0 \sim 5$  (see Fig. 4d). The phase diagram of the Pei-Hub model is similar to Fig. 4 except that the phase with dominant SS is removed and the dashed line is shifted to slightly lower  $E_F/\omega_0$ .

It is worth pointing out the intriguing possibility that, for a *quasi*-1D system with dynamically fluctuating 1D chains, or even for chains that exhibit transverse spatial fluctuations, CDW order is easily dephased, while the superconducting instability is not.<sup>22</sup> If this is the case, then the theory here predicts that it is possible for the system to support superconductivity even for the physically realistic case of  $\bar{U} \gg \lambda_{\text{Hol}}$ , and without the large amount of retardation that is required in 3D.

A number of authors have computed the phase diagram of the *spinless* Holstein model at half-filling, in the absence of el-el interactions. They often present diagrams in the  $g/\omega_0 - t/\omega_0$  plane (see Fig. 9). In Fig. 5, we present a phase diagram in similar units for the spinful incommensurate extended Holstein-Hubbard model.

### B. Near half-filling

If we reduce the doping level of an incommensurate system (*i.e.* move closer to half-filling), the LL-LEL phase boundary is influenced in opposite ways for the Hol-Hub compared to the Pei-Hub model. This is because a repulsive on-site  $U$  is in direct competition with the attractive on-site el-ph interaction of the Holstein model, while it cooperates with the attractive bond centered interaction of the Pei model. Therefore, for  $U > 0$ , the spin gap is enhanced by proximity to half-filling for the Pei-Hub model, and reduced for the Hol-Hub model.

We illustrate this in Fig. 6, which presents a phase diagram in the  $\bar{U}l_0 - \lambda l_0$  plane, for the case  $V = 0$ . This diagram shows the dependence of the LL-LEL phase boundary on the doping parameter

$$\delta = \frac{\ln(\mu/\omega_0)}{\ln(E_F/\omega_0)}. \quad (5)$$

Assuming the charge gap  $\Delta_c < \mu$ , the actual doping con-

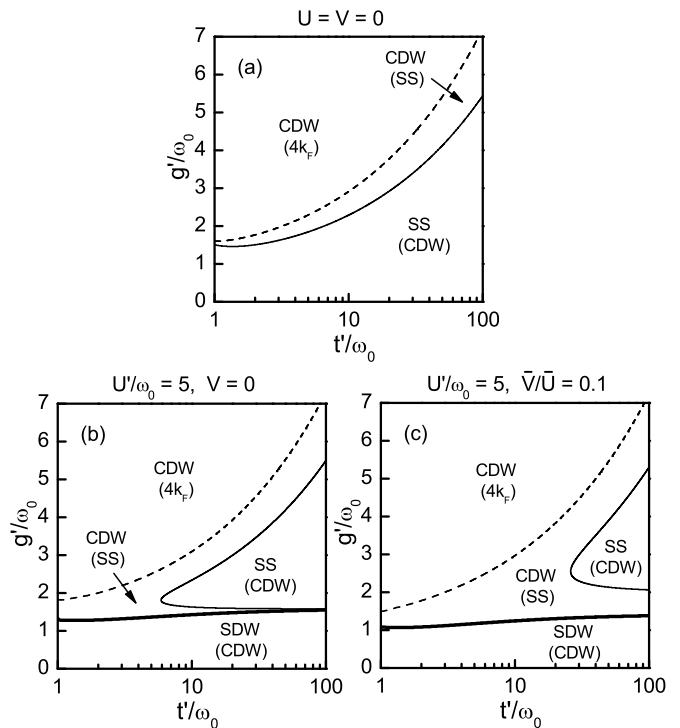


FIG. 5: Phase diagram in the  $g'/\omega_0 - t'/\omega_0$  plane of the spinful incommensurate extended Hol-Hub model for (a)  $U = V = 0$ ; (b)  $U'/\omega_0 = 5$ ,  $V = 0$ ; and (c)  $U'/\omega_0 = 5$ ,  $\bar{V}/\bar{U} = 0.1$ . Here  $g' \equiv g\sqrt{E_F/v_F}$ ,  $t' \equiv t(E_F/2t)$ , and  $U' \equiv U(E_F/v_F)$ . In (a), a spin gap is present everywhere in the phase diagram, while in (b) and (c), it is present above the thick solid line.

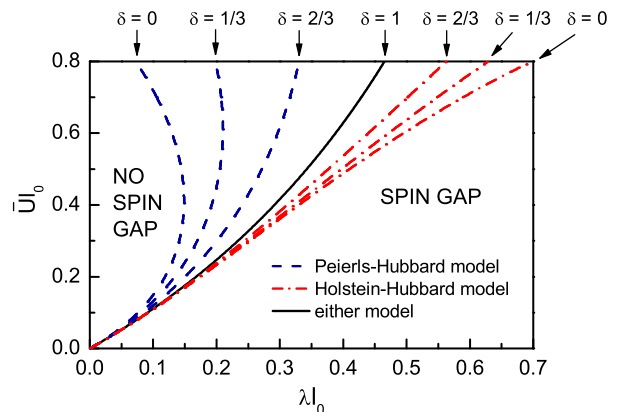


FIG. 6: Dependence of the transition line between spin-gapped and non-spin-gapped phases on the doping parameter  $\delta$  and on the electron-phonon model, for the case  $V = 0$ . For  $\mu \leq \omega_0$  (which includes the half-filled case  $\mu = 0$ ), the transition line is denoted by  $\delta = 0$ . The strongly incommensurate case ( $\mu \sim E_F$ ) is labeled by  $\delta = 1$ .  $\delta = 1/3$  and  $2/3$  are intermediate dopings, with  $\mu/\omega_0 = (E_F/\omega_0)^\delta$ . Here  $\lambda$  stands for  $\lambda_{\text{Pei}}$  in the Pei-Hub model (dashed lines) and for  $\lambda_{\text{Hol}}$  in the Hol-Hub model (dash-dotted lines). For  $\delta = 1$  (solid line), the transition line is the same for either model.

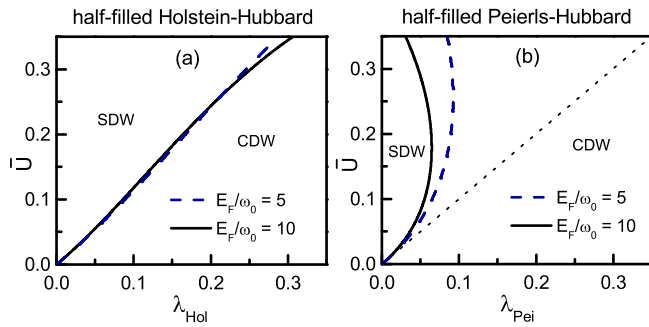


FIG. 7: Phase diagram of the (a) half-filled Hol-Hub model and (b) half-filled Pei-Hub model, both with  $V = 0$ . The dashed lines are for  $E_F/\omega_0 = 5$  and the solid lines for  $E_F/\omega_0 = 10$ . For both diagrams, a spin gap is present for the CDW phase, while a charge gap is present everywhere in the phase diagram. In (b) the dotted line, defined by  $\lambda_{\text{Pei}} = \bar{U}$ , is the inaccurate result for the phase boundary from mean field theory.<sup>24</sup>

centration  $x$  is related to  $\delta$  by

$$x = \frac{2}{\pi v_c} \mu = \frac{2\omega_0}{\pi v_c} \left( \frac{E_F}{\omega_0} \right)^\delta, \quad (6)$$

where  $v_c \approx v_F$  is the charge velocity (Eq. 35). The strongly incommensurate case  $\delta = 1$  is shown previously in Fig. 3a and Fig. 3b as a thick solid line. As we move closer to half-filling by lowering  $\delta$ , the transition line for the Pei-Hub model (dashed line) moves toward lower values of  $\lambda$ , while the transition line for the Hol-Hub model (dash-dotted line) moves toward higher values. In the weak-coupling limit assumed here, the transition line turns out to be independent of  $\mu$  if  $\mu \leq \omega_0$ . Therefore, this phase boundary is the same for half-filling ( $\mu = x = 0$ ) as for  $\delta = 0$ .

The strong doping dependence of the LL-LEL phase boundary implies that the spin gap is strongly doping dependent, as well as the SDW, CDW and SS susceptibilities. In a forthcoming paper,<sup>23</sup> we study the doping dependence of these quantities in detail.

### C. Half-filling

At half-filling, for repulsive el-el interactions, a charge gap is present for the entire phase diagram. Divergent SS is killed at half-filling. The region without a spin gap is a SDW, while the spin-gapped region is an ordered CDW. We show the half-filled phase diagram, for both models, in Fig. 7, for several values of  $E_F/\omega_0$ . The difference between the two models is substantial, with the Pei-Hub model favoring CDW more than the Hol-Hub model. In Fig. 7b, we also draw a dashed line defined by  $\lambda_{\text{Pei}} = \bar{U}$ , which is the transition line predicted by mean field theory. Such a treatment is known<sup>25</sup> to be quite inaccurate for the Pei-Hub model, as demonstrated in the

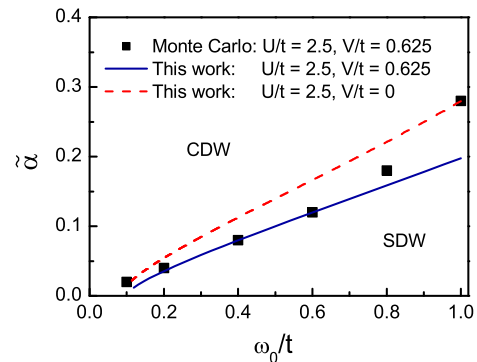


FIG. 8: Phase diagram of the half-filled Pei-Hub model. Here we compare of our result for the phase boundary (solid line) to the quantum Monte Carlo result of Ref. 26 (squares), for  $U/t = 2.5$  and  $V/t = 0.625$ . The dashed line is our result for the same  $U/t$  but with  $V = 0$ . Here  $\bar{\alpha}$  is the el-ph coupling constant in Eq. 7.

figure, since it does not take into account the dramatic renormalization of the backscattering el-ph interaction to stronger couplings. Note that the Pei-Hub phase diagram is very sensitive to  $E_F/\omega_0$ , with high values favoring a spin-gapped CDW, while the Hol-Hub phase diagram is only weakly dependent on  $E_F/\omega_0$ . It is interesting that in the Pei-Hub model (Fig. 7b), there is a maximum value of the critical el-ph coupling of about  $0.149/l_0$ , which occurs at  $\bar{U} \approx 0.411/l_0$ . (In other words, for  $\lambda_{\text{Pei}} > 0.149/l_0$ , the system is an ordered CDW for any  $\bar{U}$ .)

## IV. COMPARISON WITH OTHER WORK

Most of the phase diagrams in the present paper have not been previously computed, to our knowledge. Below, we compare our results to some phase diagrams which have been previously studied.

### A. Half-filled extended Peierls-Hubbard model

We first compare our results for the half-filled extended Pei-Hub model to recent Monte Carlo work by Sengupta, Sandvik, and Campbell<sup>26</sup> on the same model. These authors write the Hamiltonian for this model as

$$\begin{aligned} \mathcal{H}_{\text{Pei-Hub}} = & -t \sum_{i,\sigma} [1 - \tilde{\alpha}(a_i^\dagger + a_i)] (c_{i,\sigma}^\dagger c_{i+1,\sigma} + \text{H.C.}) \\ & + \omega_0 \sum_i a_i^\dagger a_i + \mathcal{H}_{UV}, \end{aligned} \quad (7)$$

where  $a_i^\dagger$  creates a phonon between sites  $i$  and  $i + 1$  and the dimensionless el-ph coupling constant is  $\tilde{\alpha} = \alpha/(t\sqrt{2M\omega_0}) = \sqrt{\pi}(\omega_0/t)\lambda_{\text{Pei}}/4$ . Following Ref. 26, we present a phase diagram in the  $\tilde{\alpha} - \omega_0/t$  plane in Fig. 8. This figure compares our result for the critical line for

$U/t = 2.5$  and  $V/t = 0.625$  (solid line) to the result in Ref. 26 for the same parameters. (In order to plot our result in these units, a value had to be assigned to the high energy cutoff  $E_F$  in the RG theory, which we took to be  $t$ . As with any weak-coupling RG method, other than the requirement that this cutoff is on the order of the Fermi energy, its precise value is somewhat arbitrary.)

The quantitative disagreement near  $\omega_0/t \sim 1$  can probably be attributed to the fact that the assumption in the RG theory of a linear electronic dispersion becomes problematic when  $\omega_0 \sim E_F$ . At lower  $\omega_0/t$ , the agreement is excellent, especially considering the moderately strong value  $\bar{U} = U/(2\pi t) \approx 0.4$ . This gives one reason to believe that the multi-step RG method is, at the very least, qualitatively accurate for physically interesting values of  $\bar{U} \sim 1$ .

In Fig. 8, we have also plotted our result for  $V = 0$  (dashed line), which can be obtained from the simple analytic expression in Eq. 53. The solid line in this figure is the only phase boundary in this paper that required numerical integration of the RG flow equations (Eqs. 14 and 15). The phase boundaries in all other plots are given by analytic expressions derived in Sec. V. Therefore, while the multi-step RG method lacks the ability of numerical methods to handle strong couplings, it is flexible and powerful in the sense that one can easily obtain simple, explicit expressions for a broad range of models at any desired band filling.

### B. Holstein model

The phase diagram for perhaps the most interesting model studied in this paper, the spinful incommensurate extended Holstein-Hubbard model, has not been computed by others, to our knowledge. A much simpler related model, which has been thoroughly explored by others, is the spinless half-filled Holstein model (without el-el interactions). We show the phase diagram for this model in Fig. 9, computed by various authors with a wide range of methods. Note that the result from the two-step RG technique (line with squares)<sup>14</sup> is in good agreement with exact numerical methods.

In order to see how Fig. 9 changes when spin is included and the system is doped away from half-filling, we have presented a diagram in similar units for the spinful incommensurate Holstein model in Fig. 5a. In order to see how it changes further with the addition of el-el interactions, we included extended Hubbard model interactions in Figs. 5b and 5c. In these diagrams, for technical reasons, we have defined  $g' = g\sqrt{E_F/v_F}$ ,  $t' = t(E_F/2t)$ , and  $U' = U(E_F/v_F)$ .

## V. METHODS AND DERIVATIONS

Here we provide more discussion of the technique and study the scaling of the coupling parameters. We also

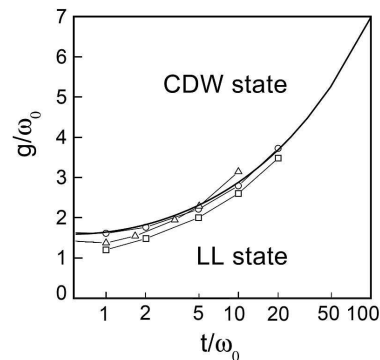


FIG. 9: Phase diagram of the spinless half-filled Holstein model from various authors, in the absence of el-el interactions. The solid line is an analytical result from Ref. 27. The line with circles and the line with squares denote the results of density matrix renormalization group<sup>28</sup> and two-step RG,<sup>14</sup> respectively. The line with triangles is the result from an exact-diagonalization method.<sup>29</sup> After Ref. 27.

derive the explicit expressions that were used to plot the phase boundaries in the figures.

### A. Field theory for the 1DEG coupled to phonons

To focus on the low energy, long wavelength physics, we work with continuum versions of Eqs. 1 and 3. The purely electronic part of our Hamiltonian is the standard continuum model of the interacting 1DEG, in which the spectrum is linearized around the left and right Fermi points. The destruction field for fermions of spin  $\sigma$  is written as a sum of slowly varying right and left moving fields:  $\Psi_\sigma = e^{ik_F x} \psi_{1,\sigma} + e^{-ik_F x} \psi_{-1,\sigma}$ . Then the kinetic energy density is

$$\mathcal{H}_0 = -iv_F \sum_{\eta,\sigma=\pm 1} \eta \psi_{\eta,\sigma}^\dagger \partial_x \psi_{\eta,\sigma}. \quad (8)$$

The important short range el-el interaction terms for a 1DEG are given in position space by the Hamiltonian density

$$\begin{aligned} \mathcal{H}_{\text{el-el}} = & g_1^0 \sum_{\sigma,\sigma'=\pm 1} \psi_{1,\sigma}^\dagger \psi_{-1,\sigma'}^\dagger \psi_{1,\sigma'} \psi_{-1,\sigma} \\ & + g_2^0 \sum_{\sigma,\sigma'=\pm 1} \psi_{1,\sigma}^\dagger \psi_{-1,\sigma'}^\dagger \psi_{-1,\sigma'} \psi_{1,\sigma} \\ & + g_3^0 [e^{i(4k_F - G)x} \psi_{-1,\uparrow}^\dagger \psi_{-1,\downarrow}^\dagger \psi_{1,\downarrow} \psi_{1,\uparrow} + \text{H.C.}] \\ & + g_4^0 \sum_{\eta,\sigma=\pm 1} \psi_{\eta,\sigma}^\dagger \psi_{\eta,-\sigma}^\dagger \psi_{\eta,-\sigma} \psi_{\eta,\sigma} \end{aligned} \quad (9)$$

where we have assumed the system is spin-rotation invariant, and the 0 superscripts are used to remind the reader that these are bare (unrenormalized) couplings. The  $g_2^0$  and  $g_4^0$  terms describe forward scattering, the former containing scattering on both left and right moving branches

and the latter containing scattering on only one branch. The  $g_1^0$  term contains backscattering from one branch to the other. The  $g_3^0$  term contains Umklapp processes and is only important when  $4k_F$  equals a reciprocal lattice vector  $G$ , *i.e.* at half-filling ( $4k_F = 2\pi$ ). For the extended Hubbard model in the continuum limit, the  $g_i^0$ 's are given by

$$\begin{aligned} g_1^0 &= g_3^0 = U - 2V', \\ g_2^0 &= U + 2V', \\ g_4^0 &= U/2 + 2V' \end{aligned} \quad (10)$$

where again  $V' \equiv -V \cos(2k_F)$ .

We incorporate el-ph interactions by defining retarded interactions  $g_{1,\text{ph}}^0$ ,  $g_{2,\text{ph}}^0$ ,  $g_{3,\text{ph}}^0$ , and  $g_{4,\text{ph}}^0$  which play the same role as the  $g_i^0$ 's except that the energy transfer is restricted to be less than a cutoff  $\omega_c$ , which is approximately the phonon frequency  $\omega_0$  ( $\omega_c$  will be defined more precisely below). This corresponds to approximating the phonon propagator as a step function of frequency, which is a good approximation for the momentum independent phonon dispersions we consider in this paper. In the Pei-Hub model, the bare el-ph couplings are given by

$$\begin{aligned} g_{1,\text{ph}}^0 &= -g_{3,\text{ph}}^0 = -\pi v_F \lambda_{\text{Pei}}, \\ g_{2,\text{ph}}^0 &= g_{4,\text{ph}}^0 = 0. \end{aligned} \quad (11)$$

For the Hol-Hub model they are

$$g_{1,\text{ph}}^0 = g_{2,\text{ph}}^0 = g_{3,\text{ph}}^0 = g_{4,\text{ph}}^0 = -\pi v_F \lambda_{\text{Hol}}, \quad (12)$$

where  $\lambda_{\text{Pei}}$  and  $\lambda_{\text{Hol}}$  are the positive, dimensionless coupling constants defined in Eq. 4. Note that the couplings  $g_{1,\text{ph}}^0$ ,  $g_{2,\text{ph}}^0$ , and  $g_{4,\text{ph}}^0$  are negative, indicating the attractive interaction induced by phonons. In the absence of el-el interactions, the sign of  $g_{3,\text{ph}}^0$  is arbitrary; likewise the sign of  $g_3^0$  is arbitrary in the absence of el-ph interactions. However, for the extended Hubbard model coupled to phonons, once the sign convention  $g_3^0 = U - 2V'$  is chosen, it is required that  $g_{3,\text{ph}}^0 > 0$  for the Pei-Hub model and  $g_{3,\text{ph}}^0 < 0$  for the Hol-Hub model.

## B. Phase diagram of the 1DEG without phonons

Before deriving the phase diagram including phonons, we briefly review the known quantum phase diagram of the 1DEG without el-ph coupling,<sup>30,31</sup> by identifying the conditions for various types of order to have divergent susceptibilities in the low temperature limit.

The sign of  $g_1^0$  determines the existence or non-existence of a spin gap: a 1DEG without el-ph coupling contains a gap to spin excitations for  $g_1^0 < 0$ , and no such gap for  $g_1^0 \geq 0$ , regardless of band filling. A charge gap is only possible at commensurate fillings.

An incommensurate 1DEG without a spin gap (Luttinger liquid), has a divergent  $2k_F$  SDW susceptibility

TABLE I: Qualitative conditions for various ordering fluctuations to dominate for an incommensurate 1DEG. See the text for quantitative conditions.

Type of Order	Dominates for <sup>a</sup>
$4k_F$ Charge Density Wave ( $4k_F$ )	$\Delta_s = 0$ , very small $K_c$
$2k_F$ Spin Density Wave (SDW)	$\Delta_s = 0$ , small $K_c$
$2k_F$ Charge Density Wave (CDW)	$\Delta_s > 0$ , small $K_c$
Triplet Superconductivity (TS)	$\Delta_s = 0$ , large $K_c$
Singlet Superconductivity (SS)	$\Delta_s > 0$ , large $K_c$

<sup>a</sup> For the Hubbard model, small  $K_c$  corresponds to repulsive interactions, large  $K_c$  to attractive interactions. The effect of a forward scattering el-ph interaction is to raise  $K_c$ , while a backscattering el-ph interaction lowers  $K_c$  and, if strong enough, causes a gap in the spin sector ( $\Delta_s > 0$ ).

TABLE II: Conditions for SDW and CDW order in a half-filled, charge-gapped 1DEG.

Type of Order	Present for
$2k_F$ Spin Density Wave (SDW)	$\Delta_s = 0$
$2k_F$ Charge Density Wave (CDW)	$\Delta_s > 0$

when the Luttinger charge exponent

$$K_c = \sqrt{\frac{2\pi v_F + 2g_4^0 + g_1^0 - 2g_2^0}{2\pi v_F + 2g_4^0 - g_1^0 + 2g_2^0}} \quad (13)$$

is less than 1, along with a logarithmically more weakly divergent  $2k_F$  CDW correlation. If  $K_c < 1/2$ , the  $4k_F$  CDW correlation is also divergent; it is less divergent than SDW and  $2k_F$  CDW for  $1/3 < K_c < 1/2$ , but becomes the dominant order for  $K_c < 1/3$ . For  $K_c > 1$ , a LL has a divergent triplet superconducting (TS) correlation and a logarithmically weaker divergent singlet superconductivity.

An incommensurate spin-gapped 1DEG (Luther-Emery liquid), is dominated by either SS or  $2k_F$  CDW correlations, depending on the value of  $K_c$ . A LEL with  $K_c < 1$  is dominated by  $2k_F$  CDW. If  $K_c < 1/2$ ,  $4k_F$  CDW is sub-dominant, while if  $1/2 < K_c < 1$ , SS fluctuations replace  $4k_F$  CDW as the sub-dominant order. For  $1 < K_c < 2$ , SS is the most divergent channel, and CDW is sub-dominant. For  $K_c > 2$ , the only divergent correlations is SS. We summarize the phase diagram of the incommensurate 1DEG, qualitatively, in Table I.

At half-filling, a 1DEG is charge gapped for  $|g_3^0| > g_1^0 - 2g_2^0$ , which for repulsive interactions is always satisfied. For  $g_1^0 < 0$ , the ground state of a charge gapped system is an ordered, spin-gapped CDW (the Peierls instability), otherwise it is a SDW with no spin gap.

### C. The multi-step RG technique

To determine the phase diagrams, we will apply the following one-loop RG flow equations<sup>9</sup>

$$\frac{dg_1}{d\ell} = -\frac{g_1^2}{\pi v_F}, \quad \frac{dg_c}{d\ell} = -\frac{g_3^2}{\pi v_F}, \quad \frac{dg_3}{d\ell} = -\frac{g_3 g_c}{\pi v_F}, \quad (14)$$

$$\frac{dg_{\pm, \text{ph}}}{d\ell} = -\frac{g_{\pm, \text{ph}}}{\pi v_F} \left( \frac{3}{2}g_1 \pm g_3 + \frac{1}{2}g_c + g_{\pm, \text{ph}} \right), \quad (15)$$

$$\frac{dg_{2, \text{ph}}}{d\ell} = \frac{dg_{4, \text{ph}}}{d\ell} = \frac{dg_4}{d\ell} = 0, \quad (16)$$

$$\frac{d\omega_c}{d\ell} = \left( 1 + \frac{g_{\pm, \text{ph}}}{\pi v_F} \right) \omega_c, \quad (17)$$

$$\frac{d\mu}{d\ell} = \mu, \quad (18)$$

with

$$g_{\pm, \text{ph}} \equiv g_{1, \text{ph}} \pm g_{3, \text{ph}}, \quad g_c \equiv g_1 - 2g_2. \quad (19)$$

These equations, which describe changes in the effective interactions when we integrate out electronic modes between the energies  $\Omega$  and  $\Omega e^{-\ell}$ , are accurate for  $E_F \gg \Omega \gg \omega_0, \mu$ . If instead  $\mu \gg \Omega \gg \omega_0$ , the same equations apply but with  $g_{3, \text{ph}} = g_3 = 0$ . From Eq. 14 we see that a repulsive  $g_1$  renormalizes in the same way as the Coulomb pseudopotential in a Fermi liquid – it is scaled to smaller values as one integrates out high energy degrees of freedom. However, in 1D the backscattering and Umklapp el-ph interactions are strongly renormalized. Furthermore, there are cross terms  $g_{\pm, \text{ph}} g_i$  in Eq. 15 which means that the scaling of the el-ph interaction is influenced by direct el-el interaction.

The multi-step RG procedure is as follows: Assuming  $\Delta_s < \omega_0$  and the system is at half-filling ( $\mu = 0$ ), we first integrate out fermionic degrees of freedom between the high energy scale  $E_F$  and the phonon energy  $\omega_0$  using Eqs. 14 and 15. Once  $\omega_0$  is reached, total effective interactions  $g_i^{\text{tot}}(\omega_0)$  at this energy scale are determined by adding the effective el-el coupling to the effective el-ph coupling

$$g_i^{\text{tot}}(\omega_0) = g_i(\omega_0) + g_{i, \text{ph}}(\omega_0). \quad (20)$$

Below this energy scale, there is no difference between retarded and instantaneous interactions, so  $g_i^{\text{tot}}$  renormalizes as a non-retarded interaction using Eq. 14 with  $g_i^{\text{tot}}(\omega_0)$  as the initial value. This method is called two-cutoff<sup>13,14</sup> or two-step RG. If the system is far enough away from half-filling such that  $\mu \sim E_F$ , the method is identical except that one sets  $g_3^0 = g_{3, \text{ph}}^0 = 0$  at the start. For the above cases, it is clear that the renormalized couplings  $g_i^{\text{tot}}(\omega_0)$  and the renormalized cutoff  $\omega_0$  play the same roll in the 1D electron-phonon system as  $g_i^0$  and  $E_F$  do in the pure 1DEG. Therefore, to determine the phase diagram of the 1DEG coupled to phonons, we can use the known phase diagram of the pure 1DEG, and simply replace the  $g_i^0$ 's there with  $g_i^{\text{tot}}(\omega_0)$ 's. For more

general fillings ( $0 < \mu < E_F$ ), a *three*-step RG method is necessary, which we will elaborate at the end of this section.

Note that  $\omega_0$  is the physical phonon frequency, which is related to  $\omega_c$  by the expression  $\omega_0 = \omega_c(\omega_0)$ , where  $\omega_c(\omega_0)$  is the renormalized value of  $\omega_c$  at the energy scale  $\omega_0$ , determined by Eq. 17. Likewise, we define  $\mu$  as the physical chemical potential relative to its value at half-filling; the bare chemical potential  $\mu^0$  is chosen such that when Eq. 18 is integrated from  $E_F$  to  $\mu$ , the renormalized value of  $\mu^0$  is  $\mu$ .

### D. Incommensurate filling

Below we derive the scaling of the coupling constants and phase diagrams for the case of strongly incommensurate filling ( $\mu \sim E_F$ ).

#### 1. Scaling of the coupling constants

Using Eqs. 14 and 15 with  $g_3 = g_{3, \text{ph}} = 0$ , we integrate out degrees of freedom between  $E_F$  and  $\omega$  with  $E_F > \omega \geq \omega_0$ , to obtain the follow effective couplings for incommensurate systems

$$g_c(\omega) = g_c^0, \quad (21)$$

$$g_1(\omega) = \frac{g_1^0}{1 + g_1^0 l}, \quad (22)$$

$$g_{1, \text{ph}}(\omega) = \left( \frac{g_{1, \text{ph}}^0}{1 + g_{1, \text{ph}}^0 Z} \right) \left( \frac{g_1(\omega)}{g_1^0} \right)^{3/2} \left( \frac{E_F}{\omega} \right)^{-g_c^0/2\pi v_F} \quad (23)$$

with

$$l = (\pi v_F)^{-1} \ln(E_F/\omega), \quad (24)$$

$$Z = \int_0^l dx \frac{\exp(-g_c^0 x/2)}{(1 + g_1^0 x)^{3/2}}. \quad (25)$$

In the absence of el-el interactions, the el-ph backscattering interaction  $g_{1, \text{ph}}$  scales according to  $g_{1, \text{ph}}(\omega)/g_{1, \text{ph}}^0 = (1 - |g_{1, \text{ph}}^0|l)^{-1}$ , which means that retardation acts to increase the effective  $|g_{1, \text{ph}}|$ . In Fig. 10 we study the important influence of extended Hubbard interactions on the scaling of  $g_{1, \text{ph}}$ . In the limit  $U \gg |g_{1, \text{ph}}^0|$ , the result is

$$\frac{g_{1, \text{ph}}(\omega)}{g_{1, \text{ph}}^0} \approx h(Ul) \quad (U \gg |g_{1, \text{ph}}^0|), \quad (26)$$

where for future convenience we defined

$$h(x) = \frac{\exp(G_c x/2)}{(1 + G_1 x)^{3/2}}, \quad (27)$$

$$G_1 = 1 - 2(\bar{V}/\bar{U}), \quad (28)$$

$$G_c = 1 + 6(\bar{V}/\bar{U}). \quad (29)$$

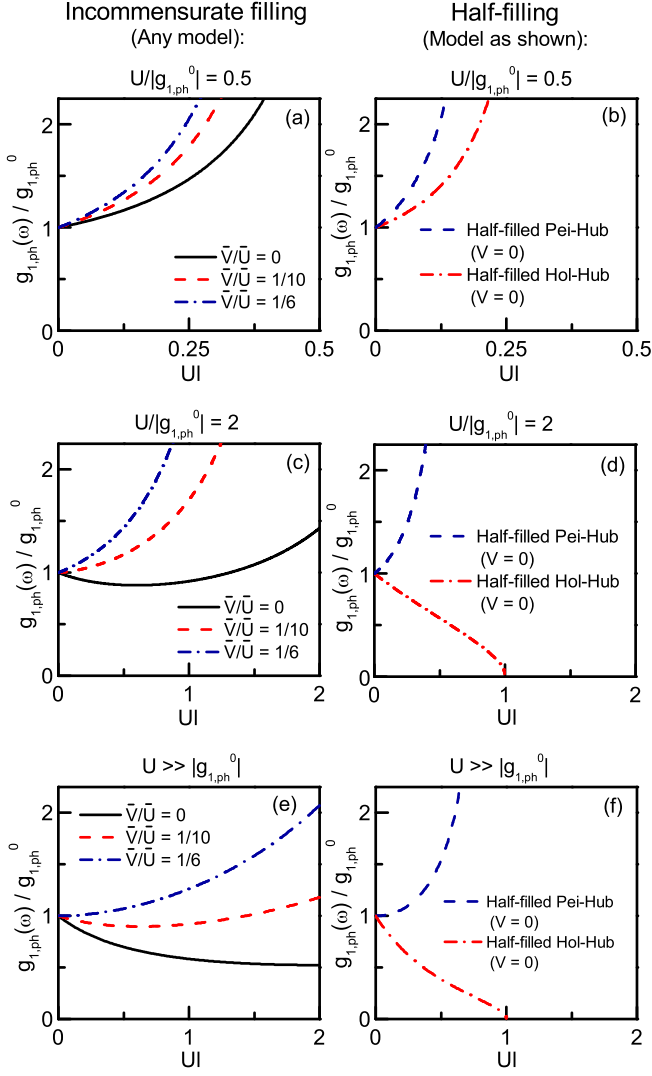


FIG. 10: The effective backscattering el-ph coupling  $g_{1,\text{ph}}(\omega)$  versus  $Ul \equiv (U/\pi v_F) \ln(E_F/\omega)$  for  $\omega > \omega_0$ . Panels (a), (c), and (e) are for strongly incommensurate systems, while (b), (d) and (f) are for the half-filled Pei-Hub and Hol-Hub models with  $V = 0$ . For each panel, the ratio of the Hubbard repulsion  $U$  to the bare backscattering el-ph coupling  $g_{1,\text{ph}}^0$  is held fixed at the value indicated.

We plot  $h(Ul)$  in Fig. 10e. Note that the scaling is very sensitive to the parameter  $\bar{V}/\bar{U}$ . For  $\bar{V}/\bar{U} < 1/6$ ,  $h(Ul)$  decreases with increasing  $Ul$  for small  $Ul$ . Therefore, in the presence of a well screened el-el repulsion that is strong compared to the bare el-ph backscattering, it is possible to have  $|g_{1,\text{ph}}(\omega_0)| < |g_{1,\text{ph}}^0|$ , provided that  $E_F/\omega_0$  is not too big. Since reducing  $|g_{1,\text{ph}}|$  causes  $K_c$  to increase, in some cases the SS susceptibility can be enhanced by increasing the el-el repulsion! This is why, in Figs. 3 and 4 for  $\bar{V}/\bar{U} = 0$ , it is possible to move from the phase with sub-dominant  $4k_F$  CDW to the phase with sub-dominant SS by increasing  $U$ . The driving force for this suppression of  $|g_{1,\text{ph}}|$  is the  $g_{\pm,\text{ph}}g_1$  cross term in Eq.

15. However, for  $\bar{V}/\bar{U} \geq 1/6$ ,  $g_{1,\text{ph}}(\omega)/g_{1,\text{ph}}^0$  is always an increasing function of  $Ul$  (assuming  $\bar{V}/\bar{U}$  is held fixed). The driving force for this increase is the  $g_{\pm,\text{ph}}g_c$  term in Eq. 15.

In real materials, one typically expects  $\bar{V}/\bar{U} \sim 1/4$ , in which case  $|g_{1,\text{ph}}(\omega_0)| > |g_{1,\text{ph}}^0|$  or even  $|g_{1,\text{ph}}(\omega_0)| \gg |g_{1,\text{ph}}^0|$ . The requirement for a spin gap is  $|g_{1,\text{ph}}(\omega_0)| > g_1(\omega_0)$ . (For repulsive el-el interactions,  $0 < g_1(\omega_0) < g_1^0$ .) In many case, only a small amount of retardation is necessary to obtain  $|g_{1,\text{ph}}(\omega_0)| \gg |g_{1,\text{ph}}^0|$ . Therefore, a slightly retarded el-ph interaction can cause a spin gap, and possibly a divergent superconducting susceptibility, even when the bare interactions are predominantly repulsive ( $|g_{1,\text{ph}}^0| \ll g_1^0$ ).

## 2. Luttinger liquid to Luther-Emery liquid transition

The phase boundary between the LL and LEL phases is given by the condition  $g_1^{\text{tot}}(\omega_0) = 0$ . Using this with Eqs. 10, 11, and 12, we find that for the extended Pei-Hub or the extended Hol-Hub models, the critical el-ph coupling at this transition is

$$\lambda_{\text{Pei}}^{\text{gap}} = \lambda_{\text{Hol}}^{\text{gap}} = \bar{U} \left[ \frac{\exp(G_c \bar{U} l_0 / 2)}{G_1 \sqrt{1 + G_1 \bar{U} l_0}} + f(\bar{U} l_0) \right]^{-1} \quad (30)$$

(LL-LEL transition)

where we defined

$$f(y) = \int_0^y dx h(x). \quad (31)$$

When  $\lambda_{\text{Pei}} > \lambda_{\text{Pei}}^{\text{gap}}$  or  $\lambda_{\text{Hol}} > \lambda_{\text{Hol}}^{\text{gap}}$ , the ground state of the incommensurate 1DEG is a spin-gapped LEL, otherwise it is a gapless LL. We plot  $\lambda_{\text{Pei}}^{\text{gap}} = \lambda_{\text{Hol}}^{\text{gap}}$  in Figs. 1 and 2. They are also shown in Figs. 3, 4, and 5 as a thick solid line. Note that in Fig. 2 we used that the scaled critical couplings  $\lambda_{\text{Hol}}^{\text{gap}} l_0$  and  $\lambda_{\text{Pei}}^{\text{gap}} l_0$  depend on only two parameters:  $\bar{U} l_0$  and  $\bar{V}/\bar{U}$ .

## 3. Susceptibilities and spin gap in the LEL phase

In the LEL phase, the low temperature susceptibilities for SS and  $2k_F$  CDW are given by  $\chi_{\text{SS}} \propto \Delta_s T^{1/K_c^{\text{eff}}-2}$  and  $\chi_{\text{CDW}} \propto \Delta_s T^{K_c^{\text{eff}}-2}$  respectively, where  $\Delta_s$  is the spin gap,  $T$  is the temperature, and  $K_c^{\text{eff}}$  is the effective Luttinger charge exponent after integrating out states between  $E_F$  and  $\omega_0$ :

$$K_c^{\text{eff}} = \sqrt{\frac{2\pi v_F + 2g_4^{\text{tot}} + g_c^{\text{tot}}(\omega_0)}{2\pi v_F + 2g_4^{\text{tot}} - g_c^{\text{tot}}(\omega_0)}} \quad (32)$$

with

$$g_c^{\text{tot}}(\omega_0) = g_c^0 + g_{1,\text{ph}}(\omega_0) - 2g_{2,\text{ph}}^0, \quad (33)$$

$$g_4^{\text{tot}} = g_4^0 + g_{4,\text{ph}}^0. \quad (34)$$

Below the energy scale  $\omega_0$ ,  $g_c^{\text{tot}}$  (and therefore  $K_c$ ) is unrenormalized. Note that the effective charge and spin velocities are also renormalized due to phonons, the former of which is

$$v_c = (2\pi)^{-1} \sqrt{[2\pi v_F + 2g_4^{\text{tot}}]^2 - [g_c^{\text{tot}}(\omega_0)]^2}. \quad (35)$$

For the case  $-1 < g_1^{\text{tot}}(\omega_0) < 0$ ,  $\Delta_s$  is determined by the energy scale below  $\omega_0$  at which the RG analysis breaks down because the effective  $g_1^{\text{tot}}/\pi v_F$  has grown to -1. Since

$$g_1^{\text{tot}}(\omega) = \frac{g_1^{\text{tot}}(\omega_0)}{1 + [g_1^{\text{tot}}(\omega_0)/\pi v_F] \ln(\omega_0/\omega)} \quad (\omega < \omega_0), \quad (36)$$

this gives

$$\Delta_s = \omega_0 e \exp(-1/\lambda^*), \quad (37)$$

with  $\lambda^* \equiv -g_1^{\text{tot}}(\omega_0)/\pi v_F > 0$ . For  $g_1^{\text{tot}}(\omega_0) > 0$ ,  $g_1^{\text{tot}}(\omega) \rightarrow 0$  as  $\omega \rightarrow 0$ , therefore  $\Delta_s = 0$ .

#### 4. Competition between SS and CDW in the Hol-Hub model

The thin solid line in the incommensurate extended Hol-Hub model phase diagrams of Figs. 3, 4, and 5 which we call the ‘‘superconducting transition,’’ is determined by the condition  $K_c^{\text{eff}} = 1$ . This leads to the critical el-ph couplings

$$\lambda_{\text{Hol}}^{\text{SS},\pm} = \bar{U} \left[ H \pm \sqrt{H^2 - \frac{G_c}{2f(\bar{U}l_0)}} \right] \quad (38)$$

(superconducting transition)

with

$$H = \frac{2 - h(\bar{U}l_0)}{4f(\bar{U}l_0)} + \frac{G_c}{4}. \quad (39)$$

Eq. 38 implies that for fixed  $\bar{U}l_0 > 0$ , as long as the square root is not imaginary, there are *two* critical values of  $\lambda_{\text{Hol}}$ , given by  $\lambda_{\text{Hol}}^{\text{SS},+}$  and  $\lambda_{\text{Hol}}^{\text{SS},-}$ , for the transition between a phase with divergent  $2k_F$  CDW and subdominant SS, and a phase with divergent SS and subdominant  $2k_F$  CDW. Therefore, SS is the most divergent correlation provided  $G_c < 2f(\bar{U}l_0)H^2$  and  $\lambda_{\text{Hol}}^{\text{SS},-} < \lambda_{\text{Hol}}^{\text{SS},+}$ . Note that divergent a TS susceptibility is not present in any phase diagrams, since for repulsive el-el interactions,  $K_c^{\text{eff}} < 1$  whenever  $g_1^{\text{tot}}(\omega_0) > 0$ .

The phase boundary shown as a dashed line in Figs. 3, 4, and 5 is defined by  $K_c^{\text{eff}} = 1/2$ . For the extended Hol-Hub model, this condition results in the critical el-ph coupling

$$\lambda_{\text{Hol}}^{\text{CDW}} = \bar{U} \left[ L + \sqrt{L^2 + \frac{A}{2f(\bar{U}l_0)}} \right] \quad (40)$$

( $K_c^{\text{eff}} = 1/2$  transition)

with

$$L = \frac{4 - 5h(\bar{U}l_0)}{8f(\bar{U}l_0)} - \frac{A}{4}, \quad (41)$$

$$A = 3/\bar{U} - 9(\bar{V}/\bar{U}) - 1. \quad (42)$$

For  $\lambda_{\text{Hol}} > \lambda_{\text{Hol}}^{\text{CDW}}$ , a divergent SS susceptibility is not possible.

#### 5. Competition between SS and CDW in the Pei-Hub model

For the extended Pei-Hub model with repulsive el-el couplings,  $K_c^{\text{eff}} < 1$  always, which means a phase with dominant SS is impossible. For this model the condition  $K_c^{\text{eff}} = 1/2$  occurs at the critical el-ph coupling value

$$\lambda_{\text{Pei}}^{\text{CDW}} = \bar{U} \left[ \frac{5h(\bar{U}l_0)}{2A} + f(\bar{U}l_0) \right]^{-1} \quad (43)$$

( $K_c^{\text{eff}} = 1/2$  transition).

For  $\lambda_{\text{Pei}} > \lambda_{\text{Pei}}^{\text{CDW}}$ , the SS susceptibility is never divergent.  $\lambda_{\text{Pei}}^{\text{CDW}}$  is shown as a dashed line in Fig. 3c and 3d.

### E. Half-filling

At half-filling, Eqs. 14 and 15 can be integrated analytically if one takes  $g_c^0 = -g_3^0$ . For that case,

$$g_c(\omega) = -g_3(\omega) = \frac{g_c^0}{1 + g_c^{0l}}, \quad (44)$$

$$g_{+,\text{ph}}(\omega) = \left( \frac{g_{+,\text{ph}}^0}{1 + g_{+,\text{ph}}^0 X} \right) \left( \frac{g_1(\omega)}{g_1^0} \right)^{3/2} \left( \frac{g_c(\omega)}{g_c^0} \right)^{-1/2} \quad (45)$$

$$g_{-,\text{ph}}(\omega) = \left( \frac{g_{-,\text{ph}}^0}{1 + g_{-,\text{ph}}^0 Y} \right) \left( \frac{g_1(\omega)}{g_1^0} \right)^{3/2} \left( \frac{g_c(\omega)}{g_c^0} \right)^{3/2} \quad (46)$$

where

$$X = \int_0^l dx (1 + g_1^0 x)^{-3/2} (1 + g_c^0 x)^{1/2}, \quad (47)$$

$$Y = \int_0^l dx (1 + g_1^0 x)^{-3/2} (1 + g_c^0 x)^{-3/2} \\ = \frac{2}{(g_1^0 - g_c^0)^2} \left[ g_1^0 + g_c^0 - \frac{g_1^0 + g_c^0 + 2g_1^0 g_c^0 l}{\sqrt{(1 + g_1^0 l)(1 + g_c^0 l)}} \right], \quad (48)$$

and  $g_1(\omega)$  is given again by Eq. 22. Since our assumption of  $g_c^0 = -g_3^0$  is satisfied for the Hubbard model (with  $V = 0$ ), the above results determine the scalings of  $g_{1,\text{ph}}$  and  $g_{3,\text{ph}}$  for the Hol-Hub and Pei-Hub models, which are

$$g_{1,\text{ph}}(\omega) = g_{3,\text{ph}}(\omega) = \left( \frac{g_{1,\text{ph}}^0}{1 + g_{1,\text{ph}}^0 X'} \right) \sqrt{\frac{1 - Ul}{(1 + Ul)^3}}$$

(half-filled Holstein-Hubbard model), (49)

$$g_{1,\text{ph}}(\omega) = -g_{3,\text{ph}}(\omega) = \left( \frac{g_{1,\text{ph}}^0}{1 + g_{1,\text{ph}}^0 Y'} \right) \sqrt{\frac{1}{[1 - (Ul)^2]^3}}$$

(half-filled Peierls-Hubbard model), (50)

where  $X'$  and  $Y'$  are the values of  $2X$  and  $2Y$ , respectively, for the case  $g_1^0 = -g_c^0 = U$ :

$$X' = \frac{2}{U} \left[ 2 - 2\sqrt{\frac{1-Ul}{1+Ul}} - \arcsin(Ul) \right], \quad (51)$$

$$Y' = \frac{2l}{\sqrt{1-(Ul)^2}}. \quad (52)$$

In the absence of el-el interactions, for either model,  $g_{1,\text{ph}}(\omega)$  increases in strength as  $l$  is increased according to  $g_{1,\text{ph}}(\omega)/g_{1,\text{ph}}^0 = (1 - 2|g_{1,\text{ph}}^0|l)^{-1}$ . As shown in Fig. 10 (panels b, d, and f), turning on a small repulsive  $U$  has the opposite effect for the half-filled Pei-Hub model compared to the half-filled Hol-Hub model: for the former  $g_{1,\text{ph}}(\omega)$  increases even more rapidly with increasing  $l$  than before, while for the later  $g_{1,\text{ph}}(\omega)$  increases less rapidly than before. This is due to the bond (site) centered nature of the Peierls (Holstein) el-ph interaction, and shows up as a sign difference in  $g_{3,\text{ph}}^0$  for the two models.

For  $U \gg |g_{1,\text{ph}}^0|$ , the behavior of  $g_{1,\text{ph}}(\omega)/g_{1,\text{ph}}^0$  is given by the square roots in Eqs. 49 or 50, and is shown in Fig. 10f. In this limit, for the Hol-Hub model,  $g_{1,\text{ph}}(\omega)/g_{1,\text{ph}}^0$  is a decreasing function of increasing  $Ul$ . Since the spin gap is enhanced by a strong  $g_{1,\text{ph}}$ , and the charge gap is enhanced by a strong  $g_{3,\text{ph}}$ , we see that the off-diagonal phonon mechanism in the Pei-Hub model is more effective in enhancing both the charge and spin gap compared to the diagonal mechanism in the Hol-Hub model.

At half-filling, the transition line between CDW and SDW phases, called the Mott-Peierls transition, is determined by  $g_1^{\text{tot}}(\omega_0) = 0$ . The critical el-ph couplings that define this phase boundary are then

$$\lambda_{\text{Pei}}^{\text{GAP}} = \frac{\bar{U} \sqrt{1 - (\bar{U}l_0)^2}}{(1 - \bar{U}l_0)^{-1} + 2\bar{U}l_0} \quad (53)$$

(Peierls-Hubbard model: Mott-Peierls transition),

$$\lambda_{\text{Hol}}^{\text{GAP}} = \bar{U} \left[ 4 - 3\sqrt{\frac{1 - \bar{U}l_0}{1 + \bar{U}l_0}} - 2 \arcsin(\bar{U}l_0) \right]^{-1} \quad (54)$$

(Holstein-Hubbard model: Mott-Peierls transition).

For  $\lambda_{\text{Pei}} > \lambda_{\text{Pei}}^{\text{GAP}}$  in the half-filled Pei-Hub model, or  $\lambda_{\text{Hol}} > \lambda_{\text{Hol}}^{\text{GAP}}$  in the half-filled Hol-Hub model, the ground state is a spin-gapped, ordered CDW. We plot  $\lambda_{\text{Pei}}^{\text{GAP}}$  in Figs. 7b and 8, and  $\lambda_{\text{Hol}}^{\text{GAP}}$  in Fig. 7a.

## F. Near half-filling

Using two-step RG, we have derived phase boundaries for the incommensurate case  $\mu \sim E_F$ , as well as the half-filled case  $\mu = 0$ . For the more general case  $0 < \mu < E_F$ , in other words at filling near but not equal to half-filling, a *three*-step RG method is necessary. The three distinct crossover scales are the high energy  $E_F$ , low energy scale  $\omega_0$ , and chemical potential  $\mu$ . As before, retarded interactions only renormalize when integrating out states between  $E_F$  and  $\omega_0$ . But now,  $g_3$  and  $g_{3,\text{ph}}$  only play a role when integrating out states at higher energies than  $\mu$  (and if  $\mu < \omega_0$ , for states between  $\mu$  and  $\omega_0$ , only  $g_3$  plays a roll).

Here we shall use this method to determine the doping dependence of the transition line between the spin-gapped and non-spin-gapped regions, for the case  $V = 0$ . In a forthcoming paper,<sup>23</sup> we study the doping dependencies of the phase boundaries separating regions with different divergent susceptibilities. First consider the case  $\omega_0 < \mu < E_F$ . The first step is to integrate out degrees of freedom between  $E_F$  and  $\mu$  using the half-filling expressions Eq. 49 or Eq. 50 (depending on the model) to determine the effective interaction  $g_{1,\text{ph}}(\mu)$ . This value is then used as the initial value  $g_{1,\text{ph}}^0$  in the incommensurate expression Eq. 23, with  $E_F$  replaced by  $\mu$ , to determine  $g_{1,\text{ph}}(\omega_0)$ . Since  $g_1$  renormalizes in the same way for the half-filled and incommensurate cases, we can just integrate from  $E_F$  to  $\omega_0$  in one step using Eq. 22. At this point, the total effective interaction  $g_1^{\text{tot}}(\omega_0) = g_1(\omega_0) + g_{1,\text{ph}}(\omega_0)$  is determined. Again, the condition  $g_1^{\text{tot}}(\omega_0) = 0$  determines the transition to a spin gap, which leads to the critical values

$$\lambda_{\text{Pei}}^{\text{Gap}} = \frac{\bar{U} \sqrt{[1 - (c\bar{U}l_0)^2]^3}}{4 + G + 2c\bar{U}l_0[3 - (c\bar{U}l_0)^2]} \quad (55)$$

(Peierls-Hubbard model),

$$\lambda_{\text{Hol}}^{\text{Gap}} = \bar{U} \left[ 4 + G \sqrt{\frac{1 - c\bar{U}l_0}{(1 + c\bar{U}l_0)^3}} - 2 \arcsin(c\bar{U}l_0) \right]^{-1} \quad (56)$$

(Holstein-Hubbard model),

where we defined

$$G = \tilde{f}(\delta\bar{U}l_0) + (1 + \bar{U}l_0)\tilde{h}(\delta\bar{U}l_0) - 4(1 + c\bar{U}l_0),$$

$$c = 1 - \delta.$$

Here  $\delta$ , defined in Eq. 5, parameterizes the doping,  $\tilde{h}(x) = e^{x/2}(1+x)^{-3/2}$ , and  $\tilde{f}(y) = \int_0^y dx \tilde{h}(x)$ . The system is spin-gapped for  $\lambda_{\text{Pei}} > \lambda_{\text{Pei}}^{\text{Gap}}$  or  $\lambda_{\text{Hol}} > \lambda_{\text{Hol}}^{\text{Gap}}$  for the Pei-Hub and Hol-Hub models, respectively.

For the case  $\mu \leq \omega_0$ , since  $g_1$  scales in the same way at all energies and does not depend on  $g_3$ , the spin gap transition line is the same as for  $\mu = 0$ , and is given by Eqs. 55 and 56 with  $\delta = 0$ . (For  $\delta = 0$ , Eqs. 55 and 56

reduce to Eqs. 53 and 54.) For  $\delta = 1$ ,  $\lambda_{\text{Pei}}^{\text{Gap}} = \lambda_{\text{Hol}}^{\text{Gap}}$ , and we recover the incommensurate LL-LEL transition (Eq. 30) with  $V = 0$ . The critical lines computed from Eqs. 55 and 56 are plotted in Fig. 6.

## VI. CONCLUSIONS

We have explored the influence of the el-ph interaction on the rich quantum phase diagram of the most theoretically well understood non-Fermi liquid, the interacting 1DEG. The backward and Umklapp scattering portions of the el-ph interaction are strongly renormalized, often toward stronger couplings, in which case the el-ph coupling can become the most important interaction in the problem. Even in the presence of strong el-el repulsion, a weak, slightly retarded el-ph interaction is capable of creating a spin gap and causing divergent superconducting and/or CDW susceptibilities (true long range order is formed when weak-coupling between 1D chains is included). The ground state is highly doping dependent, and, especially at or near half-filling, dependent on the microscopic model of the el-ph interaction. Compared to higher dimensions, the zero-temperature phase diagram is far more complex and, away from commensurate filling, contains a subtle competition between SDW, CDW, and superconductivity. The fact that direct el-el interactions strongly influence the renormalizations of the el-ph interactions adds to the complexity of the phase diagram.

We end with a few remarks on the possible relevance of these results to the cuprate high-temperature superconductors. The following experimental observations, when combined with the theory here, suggest that one should not overlook phonons as a potentially important player in the physics of these materials. There is evidence<sup>12</sup> that fluctuating stripes may be widespread in these materials, meaning it may be valid to apply 1D theory, where, as we have shown above, the effects of even a weak el-ph coupling can be important. We have also shown that, in 1D, optical phonons are generally more favorable to superconductivity than acoustic. In the cuprates, there is experimental evidence<sup>32,33,34,35</sup> for strong coupling to

an optical phonon with  $E_F/\omega_0 \sim 5$ , which is very low compared to the value  $E_F/\omega_0 \sim 1000$  in conventional metals. Unlike in conventional metals, where the el-ph interaction is unrenormalized, so superconductivity requires  $E_F \gg \omega_0$ , in 1D  $E_F \sim \omega_0$  is ideal for superconductivity: Due to the renormalization of the el-ph coupling to stronger values, in 1D  $E_F/\omega_0 \sim 5$  is often sufficient for the effective phonon induced attraction to dominate a strong el-el repulsion, thereby causing a spin gap (the superconducting pairing energy), while  $E_F \gg \omega_0$  is harmful to superconductivity because it causes the effective Luttinger exponent  $K_c^{\text{eff}}$  to drop too low.

It is worth mentioning that the ARPES spectrum of the cuprates in the nodal direction can be fit remarkably well to an exactly solvable model of a Luttinger liquid coupled to an optical phonon.<sup>6</sup> This provides further evidence that the cuprates are non-Fermi liquids, and that, for whatever reason, they may be describable with quasi-1D physics. In a forthcoming paper,<sup>23</sup> we study the strong doping dependence of the spin gap and superconducting susceptibility. There we also demonstrate that, unlike in BCS theory, the effect of changing the ion mass on  $T_c$  (the isotope effect) is strongly doping dependent for a quasi-1DEG coupled to phonons.

To conclude, the properties of the interacting 1D electron gas coupled to phonons are dramatically different from a Fermi liquid coupled to phonons. While the majority opinion remains that phonons are not responsible for pairing in the cuprates, one should keep in mind that the well known theoretical arguments that attempt to rule out phonons as the cause of high-temperature superconductivity presuppose a Fermi liquid.<sup>36</sup> Therefore, these arguments cannot be directly applied to the quasi-1D electron gas.

## Acknowledgments

I wish to acknowledge S. E. Brown for useful conversations and am grateful to S. Kivelson for many helpful suggestions. This work was supported by the Department of Energy contract No. DE-FG03-00ER45798.

<sup>1</sup> A. Lanzara, P. V. Bogdanov, X. J. Zhou, S. A. Kellar, D. L. Feng, E. D. Lu, T. Yoshida, H. Eisaki, A. Fujimori, K. Kishio, J.-I. Shimoyama, T. Noda, S. Uchida, Z. Hussain, and Z.-X. Shen, *Nature* **412**, 510 (2001).

<sup>2</sup> P. W. Anderson, *The Theory of Superconductivity in the High- $T_c$  Cuprates* (Princeton University Press, Princeton, 1997).

<sup>3</sup> D. Orgad, S. A. Kivelson, E. W. Carlson, V. J. Emery, X. J. Zhou, and Z.-X. Shen, *Phys. Rev. Lett.* **86**, 4362 (2001).

<sup>4</sup> M. Vojta, Y. Zhang, and S. Sachdev, *Int. J. Mod. Phys. B* **14**, 3719 (2000).

<sup>5</sup> T. Valla, A. V. Fedorov, P. D. Johnson, B. O. Wells, S. L. Hulbert, Q. Li, G. D. Gu, and N. Koshizuka, *Science* **285**,

2110 (1999).

<sup>6</sup> I. P. Bindloss and S. A. Kivelson, *cond-mat/0402457*.

<sup>7</sup> E. Fradkin and J. E. Hirsch, *Phys. Rev. B* **27**, 1680 (1983); J. E. Hirsch and E. Fradkin, *Phys. Rev. B* **27**, 4302 (1983).

<sup>8</sup> J. Voit and H. J. Schulz, *Phys. Rev. B* **37**, 10068 (1988); J. Voit, *Phys. Rev. Lett.* **64**, 323 (1990).

<sup>9</sup> G. T. Zimanyi, S. A. Kivelson, and A. Luther, *Phys. Rev. Lett.* **60**, 2089 (1988).

<sup>10</sup> A. J. Heeger, S. Kivelson, and J. R. Schrieffer, *W.-P. Su, Rev. Mod. Phys.* **60**, 781 (1988).

<sup>11</sup> C. Bourbonnais, in *High Magnetic Fields: Applications in Condensed Matter Physics and Spectroscopy*, edited by C. Berthier, L. P. Levy, and G. Martinez (Springer-Verlag,

- Berlin, 2002), p. 235.
- <sup>12</sup> For a recent review of the experimental evidence regarding the existence of local stripe correlations in the high-temperature superconductors, see S. A. Kivelson, I. P. Bindloss, E. Fradkin, V. Oganesyan, J. M. Tranquada, A. Kapitulnik, and C. Howald, *Rev. Mod. Phys.* **75**, 1201 (2003).
  - <sup>13</sup> G. S. Grest, E. Abrahams, S.-T. Chui, P. A. Lee, and A. Zawadowski, *Phys. Rev. B* **14**, 1225 (1976).
  - <sup>14</sup> L. G. Caron and C. Bourbonnais, *Phys. Rev. B* **29**, 4230 (1984).
  - <sup>15</sup> T. Holstein, *Ann. Phys. (NY)* **8**, 343 (1959).
  - <sup>16</sup> W. P. Su, J. R. Schrieffer, and A. J. Heeger, *Phys. Rev. Lett.* **42**, 1698 (1979).
  - <sup>17</sup> V. J. Emery, in *Highly Conducting One-Dimensional Solids*, edited by J. T. Devreese, R. P. Evrard, and V. E. van Doren (Plenum, New York, 1979), p. 247.
  - <sup>18</sup> E. Fradkin, *Field Theories of Condensed Matter Systems* (Addison-Wesley, Massachusetts, 1991).
  - <sup>19</sup> J. Voit, *Rep. Prog. Phys.* **58**, 977 (1995).
  - <sup>20</sup> A. O. Gogolin, A. A. Nersesyan, and A. M. Tsvelik, *Bosonization and Strongly Correlated Systems* (Cambridge University Press, Cambridge, 1998).
  - <sup>21</sup> A. Luther and V. J. Emery, *Phys. Rev. Lett.* **33**, 589 (1974).
  - <sup>22</sup> S. A. Kivelson, E. Fradkin and V. J. Emery, *Nature* **393**, 550 (1998).
  - <sup>23</sup> I. P. Bindloss, to be published.
  - <sup>24</sup> S. Kivelson and D. E. Heim, *Phys. Rev. B* **26**, 4278 (1982).
  - <sup>25</sup> S. A. Kivelson and M. I. Salkola, *Synth. Met.* **44**, 281 (1991).
  - <sup>26</sup> P. Sengupta, A. W. Sandvik, and D. K. Campbell, *Phys. Rev. B* **67**, 245103 (2003).
  - <sup>27</sup> Q. Wang, H. Zheng, and M. Avignon, *Phys. Rev. B* **63**, 14305 (2000).
  - <sup>28</sup> R. J. Bursill, R. H. McKenzie, and C. J. Hamer, *Phys. Rev. Lett.* **80**, 5607 (1998).
  - <sup>29</sup> A. Weisse and H. Fehske, *Phys. Rev. B* **58**, 13526 (1998).
  - <sup>30</sup> T. Giamarchi and H. J. Schulz, *Phys. Rev. B* **39**, 4620 (1989).
  - <sup>31</sup> E. W. Carlson, V. J. Emery, S. A. Kivelson and D. Orgad, to be published in *The Physics of Conventional and Unconventional Superconductors*, edited by K. H. Bennemann and J. B. Ketterson, (Springer-Verlag, Berlin), cond-mat/0206217.
  - <sup>32</sup> R. J. McQueeney, Y. Petrov, T. Egami, M. Yethiraj, G. Shirane, and Y. Endoh, *Phys. Rev. Lett.* **82**, 628 (1999).
  - <sup>33</sup> L. Pintschovius and M. Braden, *Phys. Rev. B* **60**, R15039 (1999).
  - <sup>34</sup> Guo-meng Zhao, H. Keller, and K. Conder *J. Phys.: Condens. Matter* **13**, R569 (2001).
  - <sup>35</sup> J.-H. Chung, T. Egami, R. J. McQueeney, M. Yethiraj, M. Arai, T. Yokoo, Y. Petrov, H. A. Mook, Y. Endoh, S. Tajima, C. Frost, and F. Dogan *Phys. Rev. B* **67**, 014517 (2003).
  - <sup>36</sup> The well known reasons to believe that a Fermi liquid coupled to phonons (BCS theory) always leads to low  $T_c$ 's are reviewed in Ref. 31